JACS
JOURNAL OF THE AMERICAN CHEMICAL SOCIETY
Article
pubs.acs.org/JACS

$SrFe_{0.5}Ru_{0.5}O_2$: Square-Planar Ru^{2+} in an Extended Oxide

Fabio Denis Romero,[†] Steven J. Burr,[†] John E. McGrady,[†] Diego Gianolio,[‡] Giannantonio Cibin,[‡] and Michael A. Hayward*[,†]

[†]Inorganic Chemistry Laboratory, Department of Chemistry, University of Oxford, South Parks Road, Oxford OX1 3QR, United Kingdom

[‡]Diamond Light Source Ltd., Harwell Science and Innovation Campus, Didcot OX11 0DE, United Kingdom

Supporting Information

ABSTRACT: Low-temperature topochemical reduction of the cation disordered perovskite phase $SrFe_{0.5}Ru_{0.5}O_3$ with CaH_2 yields the infinite layer phase $SrFe_{0.5}Ru_{0.5}O_2$. Thermogravimetric and X-ray absorption data confirm the transition metal oxidation states as $SrFe_{0.5}^{2+}Ru_{0.5}^{2+}O_2$; thus, the title phase is the first reported observation of Ru^{2+} centers in an extended oxide phase. DFT calculations reveal that, while the square-planar Fe^{2+} centers adopt a high-spin $S = 2$ electronic configuration, the square-planar Ru^{2+} cations have an intermediate $S = 1$ configuration. This combination of $S = 2$, Fe^{2+} and $S = 1$, Ru^{2+} is consistent with the observed spin-glass magnetic behavior of $SrFe_{0.5}Ru_{0.5}O_2$.

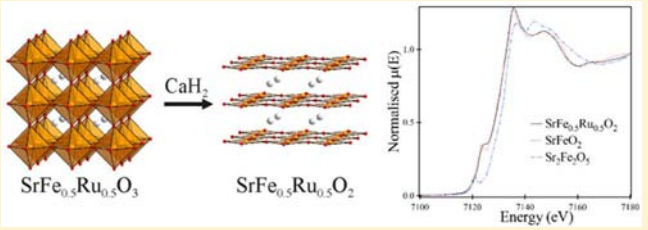

INTRODUCTION

Complex transition metal oxides have been the subject of enduring interest due to the wide variety of physical properties they exhibit. These range from correlated electronic behavior such as superconductivity[1] or magnetoresistance,[2] to the electrochemical and transport behaviors exploited in their use as electrodes and electrolytes in fuel cells[3] and lithium ion batteries,[4] to their use as heterogeneous catalysts in a number of industrially important processes.[5] The broad range of physical properties exhibited by complex transition metal oxide phases can be attributed to the presence of electrons in partially filled d-states, which interact strongly with each other via the extended metal−oxide lattice present in these materials. As a consequence the electronic structure of such materials depends on the transition metal coordination geometry and valence electron count, which together define the local transition metal electronic configuration, and the long-range metal−anion lattice structure, which defines the nature and strength of the electronic coupling between metal centers. By controlling these features of extended solids, we can tune the electronic structure of materials and thus their physical behavior.

Conventional high-temperature synthesis routes allow the preparation of a wide range of complex oxide phases. However, although this synthesis approach is widely employed, it is necessarily limited to the preparation of only the most thermodynamically stable phases in any composition range, precluding the formation of a wide range of metastable materials. By employing low-temperature "soft" synthesis techniques, which operate under conditions where kinetic rather than thermodynamic considerations dominate product selection, the range of preparable complex oxides can be extended. Recently low-temperature topochemical reduction reactions, utilizing binary metal hydrides as reducing agents, have allowed the preparation of complex oxide phases containing transition metal centers in highly unusual oxidations states and/or coordination geometries, such as square-planar Ni^+ and Co^+ and octahedral Mn^+.[6−9]

Using this strategy, Tsujimoto et al. recently reduced the cubic perovskite phase $SrFeO_{3-\delta}$ to $SrFeO_2$.[10] This Fe^{2+} oxide adopts an infinite layer structure consisting of sheets of apex-linked $Fe^{2+}O_4$ square-planes stacked with Sr^{2+} cations (Figure 1). This structure type is adopted by only a small number of complex oxide phases, such as $LnNiO_2$ (Ln = La, Nd)[6,7] and $Sr_{1-x}Ca_xCuO_2$,[11] which tend to have local transition metal valence electron counts (Ni^+, $Cu^{2+} = d^9$) which help to stabilize the square-planar transition metal coordination geometry. It is therefore somewhat surprising that $SrFeO_2$ adopts an infinite

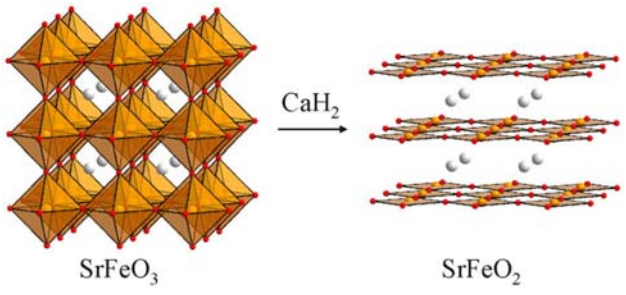

Figure 1. Topochemical reduction of $SrFeO_3$ yields the infinite layer phase $SrFeO_2$.

Received: October 4, 2012
Published: January 17, 2013

   dx.doi.org/10.1021/ja309798e | J. Am. Chem. Soc. 2013, 135, 1838−1844

layer structure, as the Fe^{2+} centers in this phase have a d^6 valence electron count which adopt a high-spin, $S = 2$, electronic configuration at ambient pressure,[12,13] providing no obvious energetic stabilization for a square-planar coordination geometry. However, even though there is no obvious stabilizing mechanism, it is clear that the d^6 electron count does play a significant role in directing the reduction reaction to form an infinite layer structure, as partially substituted $SrFe_{1-x}M_xO_{3-\delta}$ phases (M = Co, Mn) do not form infinite layer phases on reduction when $x > 0.3$.[14] In addition the infinite layer structure of the d^6, Fe^{2+} phase $SrFeO_2$ and the related Ruddlesden–Popper phase $Sr_3Fe_2O_5$ are remarkably robust, exhibiting relatively high decomposition temperatures.[10,15] In this study we utilize the robustness of the $SrFeO_2$ framework to stabilize Ru^{2+} cations within an extended oxide framework for the first time.

EXPERIMENTAL SECTION

Sample Preparation. Samples of $SrFe_{0.5}Ru_{0.5}O_3$ were prepared via a citrate gel method. Suitable stoichiometric ratios of $SrCO_3$ (99.994%), Fe_2O_3 (99.99%), and RuO_2 (99.99%, dried at 800 °C) were dissolved in a minimum quantity of 6 M nitric acid. Next, 1.333 mol equivalents of citric acid and 5 mL of analar ethylene glycol were added, and the solution was heated with constant stirring. The gels thus formed were subsequently ground into a fine powder, placed in an alumina crucible, and heated at 1 °C min^{-1} to 900 °C in air. The powders were then reground, pressed into 13 mm pellets, and heated to 1300 °C in air for two periods of 2 days. Attempts to prepare $SrFe_{1-x}Ru_xO_3$ phases with $x \neq 0.5$ were unsuccessful, resulting in the formation of mixtures of $SrRuO_3$ and $SrFeO_{3-x}$.

Samples of $SrRuO_3$ were prepared via a ceramic synthesis method.[16] Suitable stoichiometric ratios of $SrCO_3$ (99.994%) and RuO_2 (99.99%, dried at 800 °C) were ground together in an agate pestle and mortar, pressed into pellets, and heated in air for two periods of 2 days at 1150 °C. All samples were observed to be single phase by X-ray powder diffraction with lattice parameters in good agreement with literature values.[16,17]

Samples of $SrFe_{0.5}Ru_{0.5}O_2$ were prepared by reducing $SrFe_{0.5}Ru_{0.5}O_3$ with 2 mol equivalents of CaH_2 at 400 °C for two periods of 48 h in a "venting" apparatus described previously.[18] After reaction, calcium containing phases were removed from samples by washing with 4 × 100 mL aliquots of 0.1 M NH_4Cl in methanol and then a further 4 × 100 mL aliquots of clean methanol before being dried under vacuum.

Reactions between $SrRuO_3$ and two mole equivalents of CaH_2 were performed in sealed silica tubes. At reaction temperatures below 325 °C, no reaction was observed by X-ray powder diffraction. At reaction temperatures of 325 °C and above samples decomposed to form mixtures of SrO, CaO, and elemental ruthenium.

Characterization. X-ray powder diffraction data were collected from samples contained in gastight sample holders using a PANalytical X'Pert diffractometer incorporating an X'celerator position sensitive detector (monochromatic Cu $K\alpha_1$ radiation). Neutron powder diffraction data were collected using the D2B instrument (λ = 1.59 Å) at the ILL neutron source, from samples contained within vanadium cans sealed under argon with indium washers. Rietveld profile refinements were performed using the GSAS suite of programs.[19] Magnetization data were collected using a Quantum Design MPMS SQUID magnetometer. Thermogravimetric data were collected from powder samples under flowing oxygen using a Netzsch STA 409PC balance. X-ray absorption experiments were performed at the B18 beamline of the Diamond Light Source.[20] The measurements were carried out using the Pt-coated branch of collimating and focusing mirrors, a Si(111) double-crystal monochromator and a pair of harmonic rejection mirrors. The size of the beam at the sample position was approximately 600 μm (h) × 700 μm (v). XANES data were collected at the Fe K-edge (7112 eV) in transmission mode with ion chambers before and behind the sample filled with appropriate mixtures of inert gases to optimize sensitivity (I_0: 300 mbar of N_2 and 700 mbar of He, resulting in an overall efficiency of 10%; I_t: 150 mbar of Ar and 850 mbar of He, with 70% efficiency). The spectra were measured with a step size equivalent to 0.25 eV. Data were normalized using the program Athena[21] with a linear preedge and polynomial postedge background subtracted from the raw $\ln(I_t/I_0)$ data. The samples were prepared in the form of a self-supported pellet, with the thickness optimized to obtain an edge jump close to one.

Calculations. Density functional theory calculations were performed with the Siesta 2.6.8-LDAU[22,23] package using a 6×6×10 k-point grid. The PBE functional[24] was used throughout with Hubbard U values of 4.0 and 3.0 eV for Fe and Ru, respectively. The unit cell parameters were optimized to a tolerance of 0.005 eV/Å. The basis sets were of double-ζ+polarization quality, with core electrons described by norm-conserving pseudopotentials.[25] Sr semi-core levels (4s, 4p) were included in the valence space. Magnetic couplings were computed by mapping the difference between high-spin and broken-symmetry determinants onto the diagonal elements of Heisenberg-type spin Hamiltonians incorporating only nearest-neighbor interactions. Full details are given in the Supporting Information.

RESULTS

Structural and Chemical Characterization. Thermogravimetric data collected during the reoxidation of $SrFe_{0.5}Ru_{0.5}O_{3-x}$ to $SrFe_{0.5}Ru_{0.5}O_3$ (confirmed by powder X-ray diffraction) are consistent with a composition of $SrFe_{0.5}Ru_{0.5}O_2$ for the reduced phase, as shown in Figure 2.

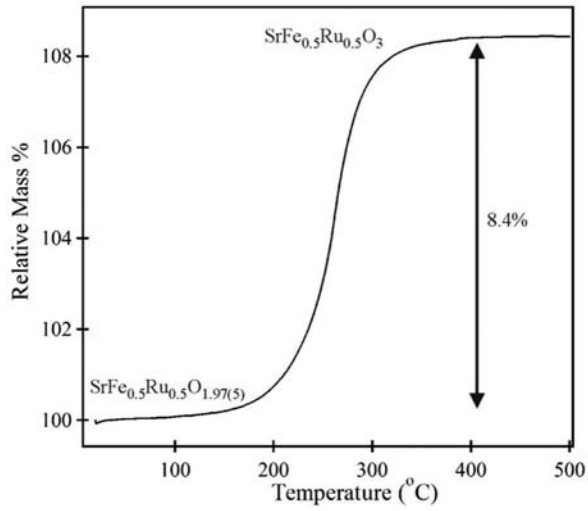

Figure 2. Thermogravimetric data collected during the reoxidation of $SrFe_{0.5}Ru_{0.5}O_2$ to $SrFe_{0.5}Ru_{0.5}O_3$.

Neutron powder diffraction data collected at room temperature from $SrFe_{0.5}Ru_{0.5}O_2$ could be readily indexed using a primitive tetragonal unit cell (a = 3.99 Å, c = 3.49 Å). Given the similarity between the lattice parameters of $SrFe_{0.5}Ru_{0.5}O_2$ and $SrFeO_2$,[10] a structural model based on the infinite layer structure of $SrFeO_2$, with a disordered 1:1 mixture of iron and ruthenium on the B-cation site, was refined against the neutron powder diffraction data collected from $SrFe_{0.5}Ru_{0.5}O_2$. The structural refinement converged readily with a good statistical fit. Close inspection of the diffraction data revealed a series of weak additional diffraction features corresponding to a small amount of CaO (2.4(2) wt%) not removed by the washing process, and so CaO was added to the structural model as a secondary phase to account for these features. A complete description of the refined structure of $SrFe_{0.5}Ru_{0.5}O_2$ is given in Table 1. Figure 3 shows a plot of the observed and calculated diffraction data from the structural refinement.

dx.doi.org/10.1021/ja309798e | J. Am. Chem. Soc. 2013, 135, 1838–1844

Table 1. Structure of $SrFe_{0.5}Ru_{0.5}O_2$ Refined against Neutron Diffraction Data Collected at 298 K

atom	x	y	z	fraction	U_{iso} (Å^2)
Sr	1/2	1/2	1/2	1	0.0041(2)
Fe/Ru	0	0	0	0.5/0.5	0.0040(1)
O	1/2	0	0	1	0.0061(2)

$SrFe_{0.5}Ru_{0.5}O_2$: $P4/mmm$, a = 3.9903(1) Å, c = 3.4978(1) Å
97.6(2) wt%

CaO: $Fm\bar{3}m$, a = 4.8152(2) Å
2.4(2) wt%

χ^2 = 2.63, wRp = 5.62%, Rp = 4.37%

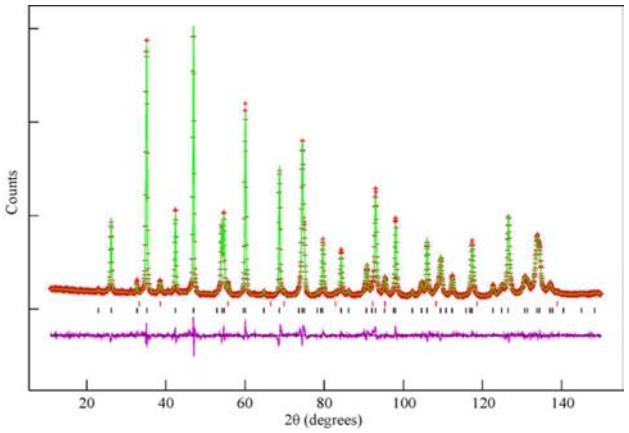

Figure 3. Observed, calculated, and difference plots from the refinement of $SrFe_{0.5}Ru_{0.5}O_2$ against neutron powder diffraction data collected at room temperature. Lower tick marks indicate peak positions for majority phase, upper tick marks for the CaO secondary phase.

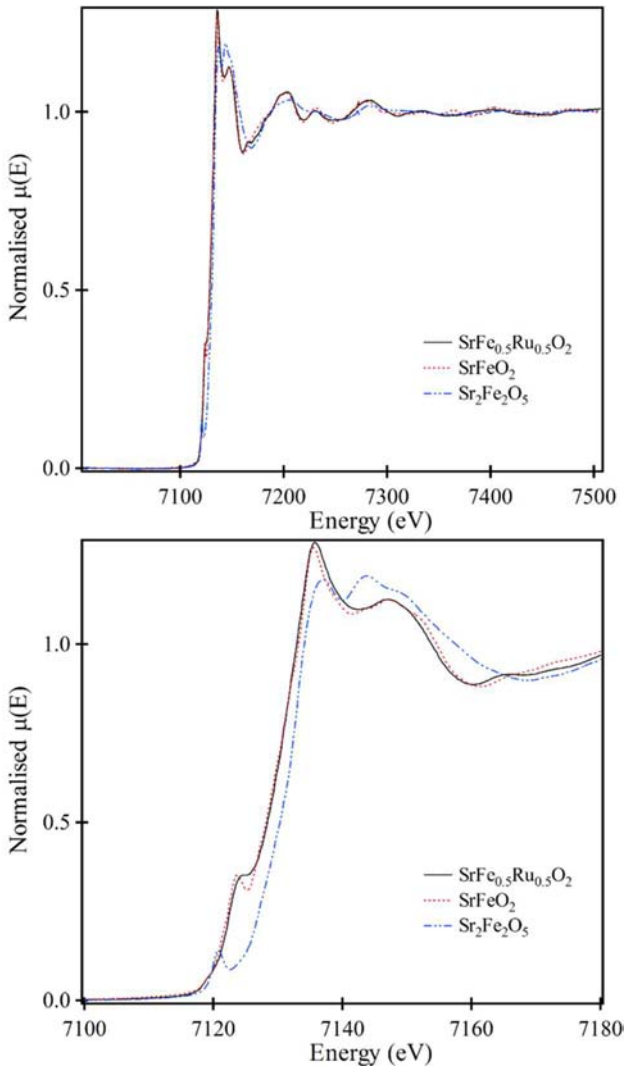

Figure 4. Normalized X-ray absorption spectra collected from the iron K-edge of $SrFe_{0.5}Ru_{0.5}O_2$, $SrFeO_2$ and $Sr_2Fe_2O_5$.

The oxygen stoichiometry of the $SrFe_{0.5}Ru_{0.5}O_2$ reduced phase defines the average transition metal oxidation state as M^{2+}; however, it does not unambiguously define the individual oxidation states of the iron and ruthenium cations. In order to resolve this ambiguity, X-ray absorption spectra were collected from the iron K-edges of $SrFe_{0.5}Ru_{0.5}O_2$, $SrFeO_2$ and $Sr_2Fe_2O_5$ as shown in Figure 4. These data reveal that the iron absorption edges of $SrFe_{0.5}Ru_{0.5}O_2$ and $SrFeO_2$ are almost identical, indicating that the iron centers in these two phases are in the same oxidation state and coordination environment (square-planar Fe^{2+}), and are distinctly different from the absorption edge of the Fe^{3+} phase $Sr_2Fe_2O_5$. Thus we can unambiguously define the transition metal oxidation states in the reduced material as $SrFe^{2+}{}_{0.5}Ru^{2+}{}_{0.5}O_2$. To the best of our knowledge this is the first time Ru^{2+} centers have been observed in an extended oxide phase.

Magnetic Characterization. Magnetization data collected from $SrFe_{0.5}Ru_{0.5}O_2$ as a function of temperature in an applied field of 100 Oe (Figure 5) show a weak divergence between zero-field-cooled and field-cooled responses in the temperature range 75 < T/K < 300. Approximate fits to the Curie–Weiss law ($\chi = C/(T - \theta) + K$) in this temperature range yield values of C = 0.369(1) cm^3 K mol^{-1}, θ = −12.3(9) K, and K = 0.00356(1) cm^3 mol^{-1}. The combination of a divergence between zero-field-cooled and field-cooled data and a small susceptibility indicates that there is strong coupling between magnetic centers even at high temperature preventing the spin-states of the Fe^{2+} and Ru^{2+} cations being deduced from the magnetization data. Below a local maximum in the zero-field-cooled data at 60 K, the zero-field-cooled and field-cooled data diverge much more strongly, indicative of a magnetic transition.

A magnetization-field isotherm collected from $SrFe_{0.5}Ru_{0.5}O_2$ at 5 K (Figure 5) exhibits weak hysteresis and is displaced significantly from the origin, indicating that the ordering event at $T \approx$ 60 K corresponds to the freezing of a spin glass. Neutron powder diffraction data collected from $SrFe_{0.5}Ru_{0.5}O_2$ at 5 K show no evidence for long-range magnetic order.

Electronic Structure. The electronic structure of $SrFeO_2$ has been described independently by both Xiang et al.[13] and Pruneda et al.,[12] who showed that the Fe^{2+} centers adopt S = 2 configurations with the d_{z^2} orbital being doubly occupied. Strong intralayer antiferromagnetic coupling between the iron centers, as anticipated based on the Goodenough–Kanamori rules,[26] then imposes an antiferromagnetic ground state. We have conducted a parallel series of calculations on $SrFe_{0.5}Ru_{0.5}O_2$ using a density functional approach (GGA +U).[27] X-ray and neutron powder diffraction data reveal that the iron and ruthenium centers are completely disordered within the ABO_2 framework. In order to model the different

dx.doi.org/10.1021/ja309798e | J. Am. Chem. Soc. 2013, 135, 1838–1844

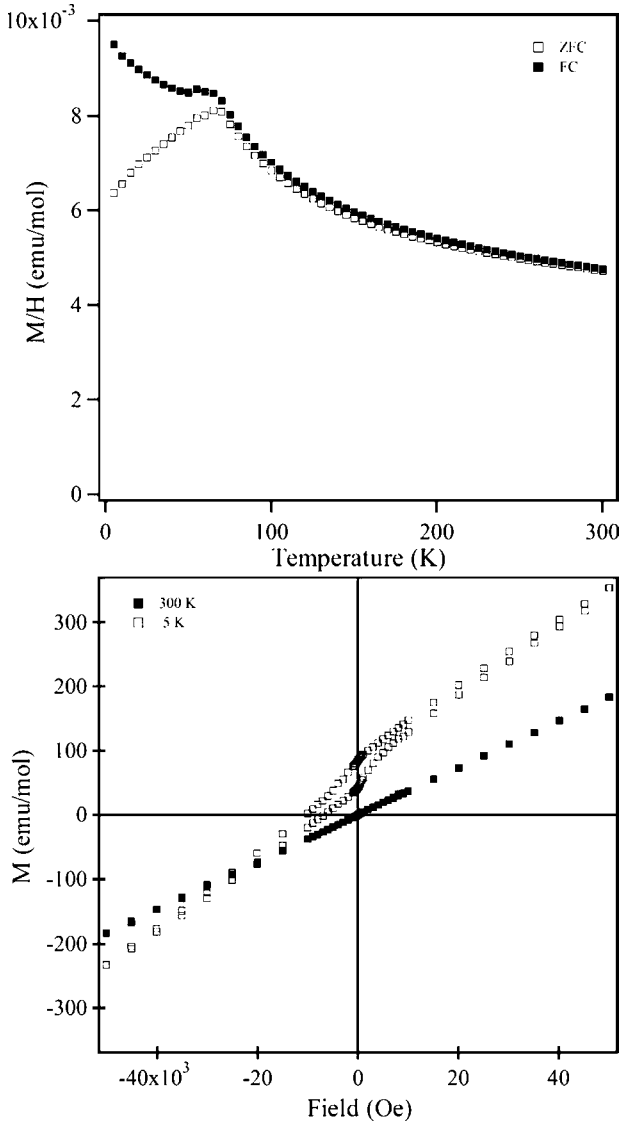

Figure 5. Zero-field-cooled and field-cooled magnetization data (top) and magnetization-field isotherms (bottom) collected from $SrFe_{0.5}Ru_{0.5}O_2$.

possible intercation interactions present in the cation disordered phase, we have considered three distinct limiting Fe/Ru ordered configurations (rock-salt, column, and planar shown in Figure 6) arranged within an $a' = \sqrt{2}a$, $c' = 2c$ expanded unit cell. While the disordered structure can be refined with a tetragonal unit cell ($P4/mmm$ space group), it remains possible that Jahn–Teller instabilities at either Fe or Ru could induce orthorhombic distortions in the three limiting ordered structures considered here. As a result we have imposed no restrictions on the lattice parameters (i.e., $a \neq b \neq c$) in the optimization procedures. Of the three structures, the rock-salt form is the most stable, although column and planar alternatives lie only 0.05 and 0.07 eV higher in energy (energies given per $SrFe_{0.5}Ru_{0.5}O_2$ formula unit). The relative thermodynamic stability of the rock-salt structure does not, however, have any direct bearing on the cation disorder as the arrangement of cations is inherited from the $SrFe_{0.5}Ru_{0.5}O_3$ perovskite parent structure. The local electronic structure at Fe and Ru proves to be independent of the cation ordering, and so we describe in detail below only the rock-salt configuration.

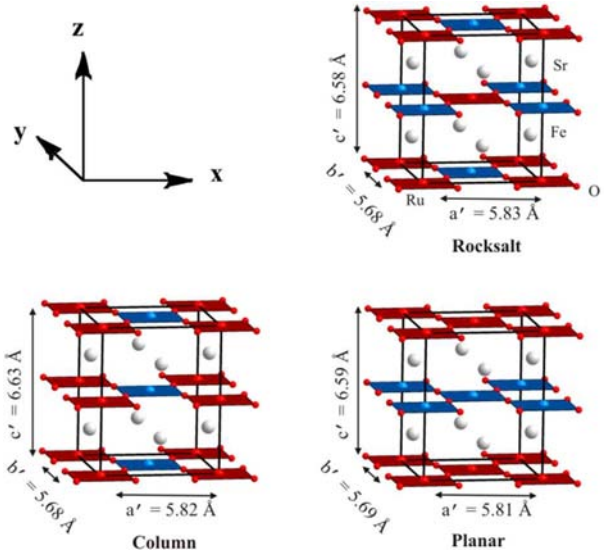

Figure 6. Optimized unit cells for the rock-salt, column, and planar configurations of $SrFe_{0.5}Ru_{0.5}O_2$.

Details of the column and planar alternatives are collected in the Supporting Information.

In the most stable electronic state of the rock-salt structure the intralayer Fe–O–Ru coupling is ferromagnetic ($J_1 = -2.39$ meV), while the interlayer coupling is weakly antiferromagnetic ($J_2 = 1.00$ meV). The partial density of states (PDOS) for Ru shown in Figure 7 confirms that the majority-spin d_{z^2}, d_{xz}, d_{yz}, and $d_{x^2-y^2}$ levels (α on Ru1, β on Ru2) lie below the Fermi level, as do minority-spin d_{yz} and d_{z2}. Note that the x and y axes are defined to lie along the unit cell vectors, as a result of which it is the d_{xy} orbital on each metal that is strongly O-M-O antibonding and not the $d_{x^2-y^2}$ as in the axis system used by Pruneda et al.[12] In contrast, minority-spin d_{xz} and $d_{x^2-y^2}$, along with both spin components of d_{xy}, lie above the Fermi level. The local configuration at Ru^{2+} is therefore a triplet, $(d_{z^2})^2(d_{xz},d_{yz})^3(d_{x^2-y^2})^1(d_{xy})^0$, consistent with Mulliken spin densities of ± 2.20 for Ru1 and Ru2, respectively. In the Fe manifold, in contrast, all five components of the majority-spin manifold (α on Fe1, β on Fe2), are occupied, along with the minority-spin d_{z^2}, giving a high-spin quintet configuration, $(d_{z^2})^2(d_{xz},d_{yz})^2(d_{x^2-y^2})^1(d_{xy})^1$ (Mulliken spin densities ± 4.08), very similar to that in the parent $SrFeO_2$ phase.[12,13] The $(d_{xz},d_{yz})^3$ configuration at ruthenium drives a small but distinct orthorhombic distortion (optimized lattice parameters: $a' = 5.83$ Å, $b' = 5.68$ Å, $c' = 6.58$ Å, $a'/b' = 1.03$), although the disorder in the crystal structure precludes the detection of such a small effect experimentally. The optimized cell parameters for the column and planar configurations are similar to those for the rock-salt analogue ($a' = 5.82$ Å, $b' = 5.68$ Å, $c' = 6.63$ Å and $a' = 5.81$ Å, $b' = 5.69$ Å, $c' = 6.58$ Å, respectively). The PDOS and Mulliken spin densities also confirm that the local electronic structure is independent of the precise arrangement of ions in the lattice: the $S = 2$ $(d_{z^2})^1(d_{xz},d_{yz})^2(d_{x^2-y^2})^1(d_{xy})^1$ and $S = 1$ $(d_{z^2})^2(d_{xz},d_{yz})^3(d_{x^2-y^2})^1(d_{xy})^0$ configurations are common to Fe and Ru, respectively, in all cases (Supporting Information, Figures S2 and S3).

DISCUSSION

Reduction of $SrFe_{0.5}Ru_{0.5}O_3$ with CaH_2 leads to the formation of the infinite-layer phase $SrFe_{0.5}Ru_{0.5}O_2$, in a process analogous

dx.doi.org/10.1021/ja309798e | J. Am. Chem. Soc. 2013, 135, 1838–1844

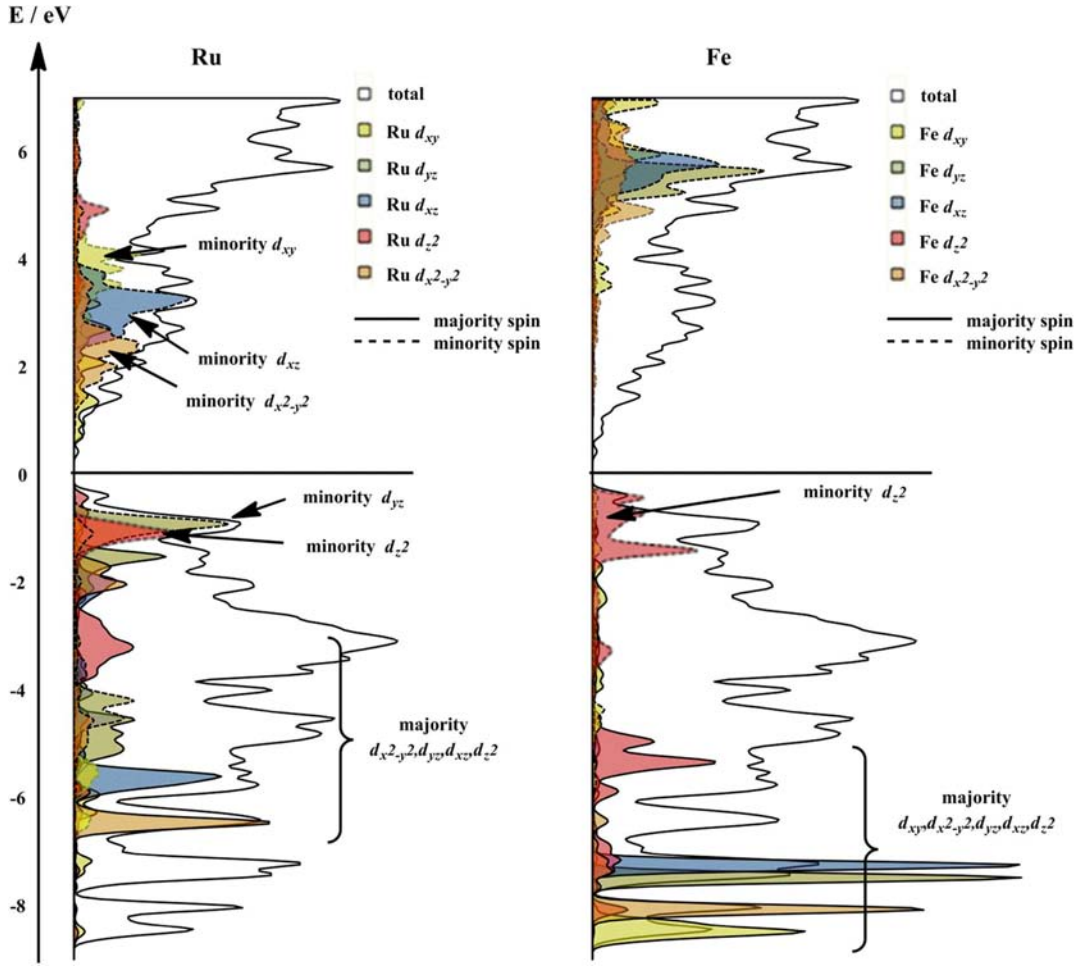

Figure 7. Computed partial density of states (PDOS) for the antiferromagnetic ground state of the rock-salt configuration of $SrFe_{0.5}Ru_{0.5}O_2$. Ru and Fe PDOS are shown on the left and right, respectively. Majority and minority-spin PDOS are shown as full and dashed lines, respectively.

to the reduction of $SrFeO_3$ to $SrFeO_2$.[10] This behavior is in strong contrast to the reduction of $SrRuO_3$, which is converted directly to elemental ruthenium and SrO, demonstrating that the presence of iron helps to stabilize the low oxidation states of ruthenium. Presumably this stabilization occurs because the extended oxide lattice couples the further reduction of the Fe^{2+} and Ru^{2+} centers—Ru^{2+} cannot be reduced to elemental ruthenium without destroying the extended oxide framework—so the endothermic reduction potential of iron can present a thermodynamic barrier to the further reduction of ruthenium centers which is not present during the reduction of $SrRuO_3$ (Fe^{2+}/Fe E° = −0.447 V; Ru^{2+}/Ru E° = +0.455 V).[28] The reduction behavior of $SrFe_{0.5}Ru_{0.5}O_3$ is also rather different from that of substituted $SrFe_{1-x}M_xO_3$ (M = Mn, Co; $x > 0.3$) phases, which are reduced to materials with non-infinite layer structures.[14] This difference clearly shows that the presence of ruthenium cations does not disrupt the structural selectivity of the low-temperature reduction reactions, reinforcing the idea that a d^6 transition metal electron count plays an important role in directing them to form products with square-planar transition metal coordination geometries.[29]

Four coordinate Ru^{2+} centers such as those seen in $SrFe_{0.5}Ru_{0.5}O_2$ are relatively rare, even in molecular complexes, due to the inherent stability of 6-coordinate $S = 0$ systems. It is possible to prepare 4-coordinate Ru^{2+} complexes by utilizing macrocyclic or chelating ligands. These compounds tend to exhibit distorted "butterfly-shaped" configurations which are stabilized by the adoption of low-spin, $S = 0$, configurations at the ruthenium center.[29] This "butterfly" distortion can be sterically suppressed by employing bulky pincer-type ligands, resulting in the formation of square-planar complexes with either $S = 1$ or $S = 0$ spin configurations depending on the π-donating properties of the ligand set.[30]

The Ru^{2+} centers present in $SrFe_{0.5}Ru_{0.5}O_2$ are observed to be square-planar by diffraction, as defined by the *P4/mmm* space group symmetry (excepting any local orthorhombic local distortion), indicating that the packing requirements of the surrounding Sr−Fe−O lattice obstruct the local "butterfly" distortions of the Ru^{2+} centers. The magnetic behavior of $SrFe_{0.5}Ru_{0.5}O_2$, discussed below, and calculations described above, indicate the ruthenium centers adopt an $S = 1$ intermediate spin state within the square-planar coordination sites of $SrFe_{0.5}Ru_{0.5}O_2$, consistent with the modest π-donating ability of the oxide ligands.

Magnetic Behavior. The parent $SrFeO_2$, exhibits antiferromagnetic order below 473 K which is attributed to strong antiferromagnetic superexchange within the Fe−O−Fe layers $\{Fe(d_{xy})^1-O(2p)-Fe(d_{xy})^1\}$ and weaker direct exchange between the layers $\{Fe(d_{xz},d_{yz})^2-Fe(d_{xz},d_{yz})^2\}$ (note axis choice as described above).[12,13] In the rock-salt configuration of $SrFe_{0.5}Ru_{0.5}O_2$, in contrast, the intralayer Ru−O−Fe coupling is ferromagnetic (J_1 = −2.39 meV, see Supporting Information)

dx.doi.org/10.1021/ja309798e | J. Am. Chem. Soc. 2013, 135, 1838−1844

because the Ru-based d_{xy} orbital is now empty $\{Fe(d_{xy})^1-O(2p)-Ru(d_{xy})^0\}$. The interlayer coupling, however, is antiferromagnetic (J_2 = 1.00 meV) due to direct $Fe(d_{xz},d_{yz})^2-Ru(d_{xz},d_{yz})^3$ exchange. The very similar structure of the Ru−O−Fe units in the column configuration also leads to ferromagnetic coupling within the layers (J_1 = −2.75 meV). In the planar alternative, however, strong σ-type $\{Fe(d_{xy})^1-O(2p)-Fe(d_{xy})^1\}$ superexchange imposes antiferromagnetic ordering within the Fe−O−Fe layers (J_1 = 1.73 meV), precisely as in $SrFeO_2$. Antiferromagnetic ordering also prevails in the Ru−O−Ru layers (J_1 = 4.77 meV), in this case due to π-type $\{Ru(d_{xz})^1-O(2p)-Ru(d_{xz})^1\}$ superexchange along the a' lattice direction. The combination of ferromagnetic Fe−O−Ru (rock-salt and column) and antiferromagnetic Fe−O−Fe and Ru−O−Ru intralayer couplings (planar) inevitably leads to magnetic frustration in any microdomain where an Ru−O−Fe unit lies directly above either Ru−O−Ru or Fe−O−Fe (Figure 8), irrespective of the sign of the interlayer coupling.

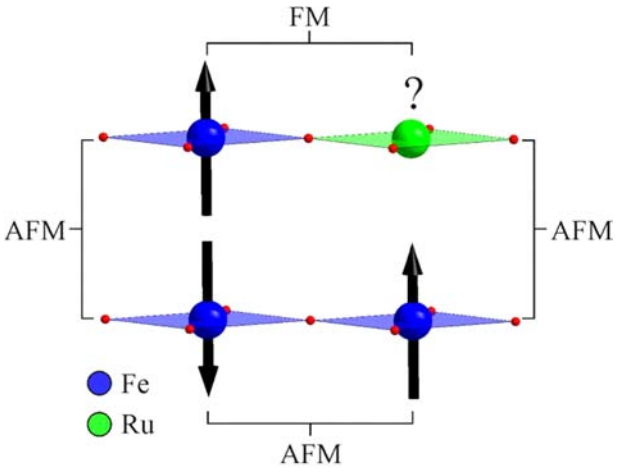

Figure 8. Frustrated ferromagnetic (FM) and antiferromagnetic (AFM) coupling interactions in a local Fe_3Ru microdomain present in $SrFe_{0.5}Ru_{0.5}O_2$.

Magnetization data collected from $SrFe_{0.5}Ru_{0.5}O_2$ show a strong divergence between zero-field-cooled and field-cooled data at 60 K, which the strongly displaced magnetization-field isotherm collected at 5 K reveals to be a spin-glass freezing transition (Figure 5). The observed spin-glass behavior is therefore a natural consequence of the disorder and the different intralayer couplings.

CONCLUSION

By utilizing the surrounding robust Sr−Fe−O framework, we have managed to impede the normally facile reduction of Ru^{2+}, and prepare $SrFe_{0.5}Ru_{0.5}O_2$, the first extended oxide phase to contain Ru^{2+} centers. Magnetization data supported by calculations indicate the square-planar Ru^{2+} centers adopt an S = 1 intermediate spin state, compared to an S = 2 spin state for the Fe^{2+} centers, consistent with the larger radial extent and hence stronger orbital-ligand interaction of 4d versus 3d metal orbitals.

Given that the isostructural all-iron phase $SrFeO_2$ undergoes a spin-state transition from S = 2 to S = 1, on the application of ∼50 GPa pressure accompanied by a phase transition from an antiferromagnetic insulating state to a ferromagnetic metallic state,[31] it seems likely that the replacement of half the S = 2, Fe^{2+} centers with S = 1, Ru^{2+} centers will significantly lower the pressure required for the analogous transition in $SrFe_{0.5}Ru_{0.5}O_2$, potentially moving it into the technologically useful range.

ASSOCIATED CONTENT

Supporting Information

Detailed descriptions of the electronic structure for $SrFeO_2$ and the column and planar forms of $SrFe_{0.5}Ru_{0.5}O_2$. This material is available free of charge via the Internet at http://pubs.acs.org.

AUTHOR INFORMATION

Corresponding Author

michael.hayward@chem.ox.ac.uk

Notes

The authors declare no competing financial interest.

ACKNOWLEDGMENTS

We thank E. Suard for assistance collecting the neutron diffraction data.

REFERENCES

(1) Bednorz, J. G.; Muller, K. A. *Z. Phys. B* **1986**, *64*, 189.
(2) *Colossal Magnetoresistance, Charge Ordering and Related Properties of Manganese Oxides*; Rao, C. N. R., Raveau, B., Eds.; World Scientific: Singapore, 1998.
(3) Kharton, V. V.; Marques, F. M. B.; Atkinson, A. *Solid State Ionics* **2004**, *174*, 135.
(4) Tarascon, J. M.; Armand, M. *Nature* **2001**, *414*, 359.
(5) Pena, M. A.; Fierro, J. L. G. *Chem. Rev.* **2001**, *101*, 1981.
(6) Hayward, M. A.; Green, M. A.; Rosseinsky, M. J.; Sloan, J. *J. Am. Chem. Soc.* **1999**, *121*, 8843.
(7) Hayward, M. A.; Rosseinsky, M. *J. Solid State Sci.* **2003**, *5*, 839.
(8) Seddon, J.; Suard, E.; Hayward, M. A. *J. Am. Chem. Soc.* **2010**, *132*, 2802.
(9) Dixon, E.; Hadermann, J.; Ramos, S.; Goodwin, A. L.; Hayward, M. A. *J. Am. Chem. Soc.* **2011**, *133*, 18397.
(10) Tsujimoto, Y.; Tassel, C.; Hayashi, N.; Watanabe, T.; Kageyama, H.; Yoshimura, K.; Takano, M.; Ceretti, M.; Ritter, C.; Paulus, W. *Nature* **2007**, *450*, 1062.
(11) Siegrist, T.; Zahurak, S. M.; Murphy, D. W.; Roth, R. S. *Nature* **1988**, *334*, 231.
(12) Pruneda, J. M.; Iniguez, J.; Canadell, E.; Kageyama, H.; Takano, M. *Phys. Rev. B* **2008**, *78*, 115101.
(13) Xiang, H. J.; Wei, S.-H.; Whangbo, M. H. *Phys. Rev. Lett.* **2008**, *100*, 167207.
(14) Seinberg, L.; Yamamoto, T.; Tassel, C.; Kobayashi, Y.; Hayashi, N.; Kitada, A.; Sumida, Y.; Watanabe, T.; Nishi, M.; Ohoyama, K.; Yoshimura, K.; Takano, M.; Paulus, W.; Kageyama, H. *Inorg. Chem.* **2011**, *50*, 3988.
(15) Kageyama, H.; Watanabe, T.; Tsujimoto, Y.; Kitada, A.; Sumida, Y.; Kanamori, K.; Yoshimura, K.; Hayashi, N.; Muranaka, S.; Takano, M.; Ceretti, M.; Paulus, W.; Ritter, C.; André, G. *Angew. Chem., Int. Ed.* **2008**, *47*, 5740.
(16) Jones, C. W.; Battle, P. D.; Lightfoot, P.; Harrison, W. T. A. *Acta Crystallogr. Sect. C: Cryst. Struct. Commun.* **1989**, *45*, 365.
(17) Battle, P. D.; Gibb, T. C.; Jones, C. W.; Studer, F. *J. Solid State Chem.* **1989**, *78*, 281.
(18) O'Malley, M.; Lockett, M. A.; Hayward, M. A. *J. Solid State Chem.* **2007**, *180*, 2851.
(19) Larson, A. C.; Von Dreele, R. B. Los Alamos National Laboratory Report LAUR 86-748, 2000.
(20) Dent, A. J.; Cibin, G.; Ramos, S.; Smith, A. D.; Scott, S. M.; Varandas, L.; Pearson, M. R.; Krumpa, N. A.; Jones, C. P.; Robbins, P. E. Presented at the 14th International Conference on X-Ray Absorption Fine Structure, 2009; Vol. *190*.
(21) Ravel, B.; Newville, M. *J. Synchrotron Radiat.* **2005**, *12*, 537.

(22) Ordejon, P.; Artacho, E.; Soler, J. M. *Phys. Rev. B* **1996**, *53*, 10441.
(23) Artacho, E.; Anglada, E.; Dieguez, O.; Gale, J. D.; Garcia, A.; Junquera, J.; Martin, R. M.; Ordejon, P.; Pruneda, J. M.; Sanchez-Portal, D.; Soler, J. M. *J. Phys.: Cond. Matter* **2008**, *20*, 064208.
(24) Perdew, J. P.; Burke, K.; Ernzerhof, M. *Phys. Rev. Lett.* **1996**, *77*, 3865.
(25) Troullier, N.; Martins, J. L. *Phys. Rev. B* **1991**, *43*, 1993.
(26) Goodenough, J. B. *Magnetism and the Chemical Bond*; Wiley: New York, 1963.
(27) When applied to $SrFeO_2$, our chosen methodology reproduces all the key features reported by Canadell and Whangbo. See Supporting Information, Figure S1.
(28) Greenwood, N. N.; Earnshaw, A. *Chemistry of the Elements*; Pergamon Press: Oxford, 1997.
(29) Lee, J. P.; Ke, Z. F.; Ramirez, M. A.; Gunnoe, T. B.; Cundari, T. R.; Boyle, P. D.; Petersen, J. L. *Organometallics* **2009**, *28*, 1758.
(30) Askevold, B.; Khusniyarov, M. M.; Herdtweck, E.; Meyer, K.; Schneider, S. *Angew. Chem., Int. Ed.* **2010**, *49*, 7566.
(31) Kawakami, T.; Tsujimoto, Y.; Kageyama, H.; Chen, X. Q.; Fu, C. L.; Tassel, C.; Kitada, A.; Suto, S.; Hirama, K.; Sekiya, Y.; Makino, Y.; Okada, T.; Yagi, T.; Hayashi, N.; Yoshimura, K.; Nasu, S.; Podloucky, R.; Takano, M. *Nat. Chem.* **2009**, *1*, 371.